


# Microglia activation and phagocytosis: relationship with aging and cognitive impairment in the rhesus monkey

Eli Shobin  · Michael P. Bowley · Larissa I. Estrada · Nadine C. Heyworth · Mary E. Orczykowski · Sherri A. Eldridge · Samantha M. Calderazzo · Farzad Mortazavi · Tara L. Moore · Douglas L. Rosene

Received: 5 October 2016 / Accepted: 7 February 2017 / Published online: 25 February 2017  
© American Aging Association 2017

**Abstract** While cognitive decline is observed in the normal aging monkey, neurons are not lost with age. Instead, frontal white matter is lost as myelin degenerates and both correlate with age-related cognitive decline. As age-related myelin damage increases, there should be an increase in clearance of damaged myelin by microglial phagocytosis. In this study, brains of behaviorally tested rhesus monkeys were assessed using unbiased stereology to quantify the density of activated microglia (LN3 antibody positive) and

phagocytic microglia (galectin-3 (Gal-3) antibody positive) in three white matter regions: the corpus callosum, cingulum bundle (CGB), and frontal white matter (FWM). LN3 cell density was significantly increased in the CGB, whereas Gal-3 cell density was significantly increased in all regions. Increases in Gal-3 cell density in the FWM were associated with cognitive impairment. In the FWM of old animals, Gal-3-positive microglia were classified by morphological subtype as ramified, hypertrophic, or amoeboid. The densities of hypertrophic and amoeboid microglia significantly correlated with cognitive impairment. Finally, microglia were double-labeled with LN3 and Gal-3 showing that 91% of Gal-3 cells were also LN3 positive, thus expressing an “activated” phenotype. Furthermore, 15% of all double-labeled cells formed phagocytic cups. Overall, these results suggest that microglia become activated in white matter with age where the majority express a phagocytic phenotype. We hypothesize that age-related phagocytic activation of microglia is a response to accumulating myelin pathology. The association of Gal-3 in the FWM with cognitive impairment may reflect regional differences in damage or dysfunction of normal clearance mechanisms.

---

E. Shobin · L. I. Estrada · N. C. Heyworth ·  
M. E. Orczykowski · S. A. Eldridge · S. M. Calderazzo ·  
F. Mortazavi · T. L. Moore · D. L. Rosene  
Department of Anatomy and Neurobiology, Boston University,  
Boston, MA 02118, USA

E. Shobin (✉)  
Graduate Program for Neuroscience, Boston University, Boston,  
MA 02118, USA  
e-mail: eshobin@bu.edu

M. P. Bowley  
Department of Neurology, Massachusetts General Hospital,  
Boston, MA 02144, USA

L. I. Estrada  
Department of Pharmacology and Experimental Therapeutics,  
Boston University, Boston, MA 02118, USA

S. A. Eldridge  
Biology Department, University of Massachusetts Dartmouth,  
Dartmouth, MA 02747, USA

T. L. Moore  
Department of Neurology, Boston University School of Medicine,  
Boston, MA 02118, USA

**Keywords** Macrophages · Aging · Myelin damage ·  
Galectin-3 · Mac-2 · Inflammation

## Introduction

A critical feature of non-neurodegenerative normal aging is a decline in cognitive function. Common

cognitive domains impaired in normal aging include memory, learning, attention, information processing, and executive function (Park and Reuter-Lorenz 2009). However, these deficits emerge at different ages and with different severity across individuals, leading to the classification of cognitively “successful” and “unsuccessful” agers (Gallagher and Burwell 1989; Moss et al. 2007). Non-human primates (NHPs) offer a model of normal aging with several advantages over studies of humans and rodents. For example, compared to human studies, the normal aging rhesus monkey offers a greater degree of experimental control, more accurate assessments of past history including health and diet, and most important, the opportunity to obtain optimally preserved brain tissue (Peters 1996). Moreover, unlike rodents which age rapidly, the rhesus monkey has a lifespan of over 30 years (Tigges et al. 1988), has a brain architecture much closer to humans and displays age-related cognitive decline in domains and at rates comparable to humans. Most important, despite the presence of amyloid (Sloane et al. 1997), monkeys do not contract Alzheimer’s disease, as there are no neurofibrillary tangles and neurons are not lost with age (Peters et al. 1998).

In searching for the neurobiological basis of age-related cognitive impairments, quantitative MRI has shown that though gray matter cortical thickness is reduced (Alexander et al. 2006; Koo et al. 2010), total gray matter volume is preserved (Wisco et al. 2008) and histological studies of gray matter have shown that neurons are not lost with age (e.g., Merrill et al. 2000; Peters et al. 1998). In contrast, both MRI and histological studies in monkeys and humans have shown that white matter volume is lost with age (Albert 1993; Guttmann et al. 1998; Peters and Rosene 2003; Tang et al. 1997; Wisco et al. 2008). Quantitative light microscopy has shown a decrease in the total length of myelinated fibers in human brain on the order of 27 to 45% with age (Mamer et al. 2003; Tang et al. 1997). Ultrastructural studies in the rhesus monkey have demonstrated age-related damage to myelin and loss of myelinated fibers in frontal white matter regions in the monkey (Bowley et al. 2010). Additionally, age-related morphological deficits in myelin can be observed at the ultrastructural level in a variety of other brain regions including the visual cortex (Peters et al. 2000), the optic nerve (Sandell and Peters 2002), fornix (Peters et al. 2010), and the anterior commissure (Sandell and Peters 2003). Finally, cognitive decline is significantly

associated with the loss of white matter volume in humans (Albert 1993) and myelin defects and degeneration in the rhesus monkey (Bowley et al. 2010).

While the cause of age-related myelin deterioration has yet to be identified, it is of interest that the accumulation of myelin debris can inhibit remyelination by reducing the differentiation of oligodendrocyte precursor cells into mature myelinating oligodendrocytes (Kotter et al. 2006). Removal of myelin debris depends upon the inflammatory and phagocytic actions of microglia, the resident macrophage of the brain (see Martinez and Gordon 2014 or Tang and Le 2015 for review). Thus, impairment in microglial function could cause or exacerbate myelin damage. Studies of the effects of age on microglia have reported that microglial activation increases with age (Henry et al. 2009). It has also been noted that activation occurs primarily in white matter rather than gray matter (Hart et al. 2012) and, in the monkey, is associated with cognitive impairment (Sloane et al. 1999; for review, see Kohama et al. 2011; Peters and Kemper 2012).

Although general changes in microglia activation have been widely studied, the phagocytic capacity of these cells in aging and cognitive decline is not as well understood. Studies on peripheral immunity have shown a loss of phagocytic capacity and function in macrophages with age (Plowden et al. 2004), although this result is not consistent across all studies (Gardner et al. 1981) and may differ between inflammatory cell types (Linehan et al. 2014). Cultured macrophages from aged humans have a diminished phagocytic capacity for myelin debris (Natrajan et al. 2015), and in vivo studies have shown that the rate of remyelination is reduced in aged rodents but can be restored with an infusion of monocytes from young animals (Ruckh et al. 2012). Finally, phagocytic activation of microglia and size of microglial lysosomes increases with age in addition to an increase in microglia adjacent to and contacting myelin (Safaiyan et al. 2016). While these data suggest that phagocytic capacity of old macrophages is impaired, the reason for this functional decline is unknown. Additionally, no study has investigated whether phagocytic activation in the aging brain is related to cognitive decline.

The current study using brain samples from behaviorally characterized rhesus monkeys was designed to assess the relationship between microglial activation

and phagocytic phenotype and their associations with age-related cognitive decline. To do so, we use galectin-3 (Gal-3) antibody as a marker for phagocytic activation. Gal-3 (also known as Mac-2) is a conserved lectin involved in cell adhesion and phagocytosis in macrophages (Dumic et al. 2006). Gal-3 is expressed ubiquitously throughout the cell, cell surface, and extracellular space and contains a C-terminal carbohydrate recognition binding domain important for cell adhesion and phagocytosis (Pugliese et al. 2015). Gal-3 is selectively upregulated in phagocytic macrophages (Elliott et al. 1991) and transgenic mice deficient in Gal-3 have reduced phagocytic ability (Sano et al. 2003). Gal-3 also is necessary for the microglial response to myelin degeneration (Hoyos et al. 2014). Additionally, we used the LN3 antibody which recognizes the HLA-DR major histocompatibility complex class II receptor to mark activated macrophages that could be either pro- or anti-inflammatory (Conde and Streit 2006). We also used double-label immunofluorescence to determine if the phagocytic priming of activated microglia changes with age or is associated with cognitive decline. The overall goal was to test the hypothesis that dysfunctional age-related phagocytic activation in the brain of behaviorally tested rhesus monkeys is related to microglial activation and cognitive impairment.

## Materials and methods

### Subjects

Brain tissue from 44 rhesus monkeys was used in this study. This tissue had been collected and stored as part of an NIA-funded Program Project (“Neural Substrates of Cognitive Decline in Aging Monkeys,” P01-AG000001) and a Research Project (“Histopathology, Neuroimaging and Mechanisms of Myelin Damage in Aging Monkey Brain,” R01-AG043640). Of the monkeys used in this study, 38 were originally obtained from the Yerkes National Primate Research Center at Emory University in Atlanta, while 6 animals came from other research centers (see Table 1). Prior to selection, health records were screened with strict health criteria to exclude any possible confounding clinical diseases or experimental manipulations that could impact normal aging by affecting the brain or behavior.

Based on tissue availability, monkeys were divided between experiments for activated microglia using LN3

( $N = 19$ ) and phagocytic microglia using Gal-3 ( $N = 30$ ). Six monkeys overlapped between studies (see Table 1). Prior studies of rhesus monkey survival and of cognitive decline suggest that, relative to humans, the rhesus monkey ages at an approximate ratio of 1 year for every three human years (Tigges et al. 1988). As such, animals for each experiment were divided into groups of young adult (ages 5.0–9.9 at euthanasia), middle-aged (ages 10.0–19.9 at euthanasia), and old (ages 20+ at euthanasia). While the young and old groups have a relative balance of males and females, there were insufficient males to balance the middle-aged subject group in each experiment. Table 1 details subjects by age at euthanasia and experiment. Although stratifying animals by age range allows for easy classification of each animal, in statistical analyses, age was also used as a continuous variable in regression analyses to identify changes that occur across the lifespan.

### Behavioral testing

Upon entering the study, all monkeys received a battery of behavioral tests that took place over a 3- to 6-month period and was completed approximately 1 to 2 months before euthanasia. These tests assess a variety of cognitive domains. Acquisition of the delayed non-match to sample (DNMS) task is a measure of rule learning. Assessment of extended delays on DNMS (120 and 600 s) test recognition memory. The Delayed Recognition Span Task assesses working memory capacity in both spatial and object modalities. Finally the Category Set Shifting Task (CSST) assesses executive function including set shifting. Details of these tasks can be found elsewhere (Herndon et al. 1997; Moore et al. 2005).

Initial inspection of how these tests compared to our measures of microglial reactivity indicated associations with measures of DNMS and DRST but not with CSST measure. Interestingly, a principal component analysis (Herndon et al. 1997) had demonstrated that a subset of DNMS and DRST measures were the best predictors of cognitive aging. These have been compiled into a z-score which designated the cognitive impairment index (CII) and has proven useful in comparing cognitive status with a variety of neurobiological endpoints (e.g., Peters et al. 1998). To avoid multiple comparison problems, the CII was used in all comparisons in this study. Table 1 presents detailed information on the CII for all subjects in the present study.

**Table 1** Subjects list for rhesus monkeys used in each study

Subject	Origin	Age at euthanasia	Sex	Age group	CII score	LN3 staining	Gal-3 staining
AM204	Yerkes	6.1	M	Y	-0.82		+
AM188	Yerkes	6.5	F	Y	0.36	+	+
AM299	Yerkes	7.1	F	Y	0.85		+
AM222	Yerkes	7.4	M	Y	0.87		+
AM132	Yerkes	7.5	M	Y	0.35	+	
AM093	Yerkes	7.6	M	Y	-0.09	+	
AM198	Yerkes	7.8	F	Y	-0.96	+	
AM128	Yerkes	7.9	M	Y	2.89	+	
AM296	Yerkes	8.7	M	Y	0.77		+
AM255	Yerkes	9.5	F	Y	0.12		+
Young	Average age (std dev)	7.4 years (0.8)			Average CII (std dev) 0.43 (1.1)		
AM214	Yerkes	10.7	F	MA	1.20		+
AM295	Yerkes	10.8	M	MA	1.52		+
AM066	Yerkes	11.2	F	MA	0.79	+	
AM194	Yerkes	11.9	F	MA	2.26	+	+
AM138	Boston VA	12.1	M	MA	NA	+	
AM195	Yerkes	12.1	F	MA	0.03		+
AM291	Yerkes	13.7	F	MA	1.17		+
AM278	Yerkes	15.3	F	MA	2.68		+
AM215	Tulane	16.6	M	MA	3.89		+
AM257	Yerkes	17.6	F	MA	1.56		+
AM190	Yerkes	18.0	F	MA	1.53	+	+
AM250	Yerkes	18.0	F	MA	6.01		+
AM274	Yerkes	18.3	F	MA	2.28		+
AM153	Boston VA	19.5	M	MA	1.00	+	
AM125	Yerkes	19.8	F	MA	3.13	+	
AM124	Yerkes	19.9	M	MA	0.94	+	
Middle-aged	Average age (std dev)	14.7 years (3.5)			Average CII (std dev) 2.0 (1.5)		
AM256	Yerkes	20.7	F	O	1.93		+
AM200	Yerkes	21.0	F	O	4.14		+
AM286	Yerkes	22.4	F	O	1.43		+
AM208	Yerkes	22.7	M	O	1.09		+
AM282	Yerkes	23.0	M	O	4.20		+
AM179	Univ Pittsburgh	23.6	F	O	6.99		+
AM189	Yerkes	24.5	M	O	2.90	+	
AM064	Stanford	24.9	M	O	0.43	+	
AM090	Yerkes	25.0	F	O	1.03	+	
AM284	Yerkes	25.4	M	O	1.47		+
AM220	Yerkes	25.7	F	O	8.77		+
AM110	Yerkes	25.8	M	O	7.93		+
AM298	Yerkes	26.7	M	O	1.28		+

**Table 1** (continued)

Subject	Origin	Age at euthanasia	Sex	Age group	CII score	LN3 staining	Gal-3 staining
AM275	Yerkes	27.8	F	O	1.60		+
AM104	Yerkes	29.0	F	O	2.15	+	+
AM180	Univ Pittsburgh	29.6	F	O	3.51	+	+
AM121	Yerkes	30.2	M	O	12.37	+	+
AM119	Yerkes	31.0	F	O	2.69	+	
Old	Average age (std dev)	24.9 years (3.0)			Average CII (std dev)	3.67 (3.3)	

### Age and cognitive impairment across experiments

Subjects from each experimental cohort were compared to ensure similarities between groups. As age is normally a predictor for cognitive impairment, the entire cohort ( $N = 44$ ) was first analyzed using regression analysis and results showed that increases in age significantly predicted increases in CII in this cohort ( $F(1,41) = 16.19$ ,  $p \leq 0.0005$ ,  $R^2 = 0.266$ ). As shown in Fig. 1, linear regression demonstrated a significant direct relationship between age and CII in each of the subsets of subjects used for Gal-3 studies ( $F(1,27) = 13.10$ ,  $p \leq 0.001$ ,  $R^2 = 0.320$ , Fig. 1a) and LN3 studies ( $F(1,16) = 5.98$ ,  $p \leq 0.05$ ,  $R^2 = 0.227$ , Fig. 1b). As one subject (AM121) with a very large CII appeared to drive the correlation between CII and age in the LN3 cohort, the CII of the LN3 subjects were tested for outliers using a multiple of 1.5 times the interquartile range to determine a cutoff of CII score 6.32. Thus, AM121 (CII score of 12.37) was removed, and the regression still demonstrated that age predicted CII ( $F(1,15) = 6.41$ ,  $p \leq 0.05$ ,  $R^2 = 0.253$ ). As the

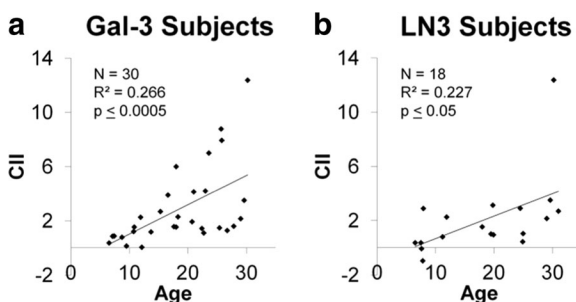


**Fig. 1** For both cohorts of the subjects in the Gal-3 analysis (a) and those in the LN3 analysis (b), cognitive impairment index (CII) scores increase significantly with age. There is a very impaired outlier (AM121) in b that drives the LN3 effect, but, even with this subject removed, the increase in CII with age is still significant ( $R^2 = 0.253$ ,  $p \leq 0.05$ )

inclusion of AM121 did not impact the significance of the correlation between age and CII score, this animal was included in all analyses unless otherwise stated.

### Brain perfusion and tissue section preparation and storage

Approximately 1 to 2 months after the conclusion of behavioral testing, monkeys were deeply anesthetized with sodium pentobarbital and perfused transcardially through the aorta with Krebs Henseleit buffer, pH 7.4 at 4 °C for 5 min while fresh tissue samples were harvested. This was followed immediately by perfusion with 4% buffered paraformaldehyde (pH 7.4, 37 °C) for 10 min. Immediately following perfusion, the brain was blocked, in situ, in the coronal stereotactic plane, removed from the skull and placed in the same paraformaldehyde fixative overnight at 4 °C. It was then cryoprotected by successive incubations in 0.1 M phosphate buffer containing first 10% glycerol with 2% DMSO and then buffer with 20% glycerol and 2% DMSO until the brain equilibrated (Rosene et al. 1986). It then was flash frozen in isopentane at  $-75$  °C after which it was stored at  $-80$  °C until it was cut on a freezing microtome into ten interrupted series of 30- $\mu$ m-thick sections. Sections were collected in buffer with 15% glycerol as a cryoprotectant, equilibrated overnight at 4 °C, and then frozen and stored at  $-80$  °C until removed and thawed for immunohistochemistry.

### Immunohistochemistry

To eliminate confounds in processing, sections for all subjects to be stained with an antibody were removed from  $-80$  °C storage at the same time, rapidly thawed to room temperature and “batch processed” together in the same reagents for the same time to facilitate quantitative

analyses across subjects. For LN3 staining, six to ten sections per animal were stained at section intervals of approximately 1200  $\mu\text{m}$ . For Gal-3 staining, four to seven sections per animal were stained at section intervals of approximately 2400  $\mu\text{m}$ . Once thawed, sections were washed three times in 0.05 M Tris-buffered saline (TBS, pH 7.6) to remove the glycerol. Immunohistochemistry protocols were optimized as described by Hoffman et al. (2016). To break cross-links formed during fixation, antigen retrieval was performed by incubating the sections in 10 mM citrate buffer (pH 6.0) in a microwave tissue processor (PELCO Biowave, Ted Pella, Inc., Redding, CA) for 5 min at 550 W and 40 °C, followed by incubation in the same buffer at room temperature for 1 h on a rocking platform. Sections were again washed in TBS (3  $\times$  5 min), then incubated with 3% buffered hydrogen peroxide for 30 min to quench endogenous peroxidases. Next, tissue was washed with TBS (3  $\times$  5 min) and blocked with SuperBlock (Life Technologies, Grand Island, NY) or 10% normal goat serum in TBS (LN3 tissue only) for 1 h. Primary antibodies were diluted 1:700 (mouse IgG1 anti-Gal-3, Abcam, Cambridge, MA) or 1:10 (mouse IgG2b anti-LN3, MP Biomedicals, Santa Ana, CA) in TBS containing 0.5% SuperBlock (or 2% normal goat serum for LN3 tissue) and 0.3% Triton-X. As a control, a few sections from various animals were placed in carrier solution (TBS containing 0.5% SuperBlock/2% normal goat serum and 0.3% Triton-X) but omitting primary antibody. For tissue in Gal-3 primary antibody, sections were microwaved in primary antibody or carrier solution for 5 min at 250 W and 30 °C. In both experiments, incubation in primary then proceeded on a rocking platform at 4 °C for 40 h.

After the primary antibody incubation, tissue was washed with TBS (3  $\times$  5 min) and incubated for 1 h in secondary antibody containing goat anti-mouse (Vector Laboratories, Burlingame, CA) diluted 1:600 in buffer containing 0.5% SuperBlock/2% normal goat serum and 0.3% Triton-X. Tissue labeled with Gal-3 was also microwaved for 5 min at 250 W and 30 °C in secondary antibody. Following the secondary antibody incubation, tissue was washed with TBS (3  $\times$  5 min) and incubated with avidin-biotin complex using Vectastain ABC kit (Vector Laboratories, Burlingame CA) for 1 h. Tissue was washed with TBS (3  $\times$  5 min), then exposed to a chromogen solution containing 0.5 mM 3,3'-diaminobenzidine (Sigma-Aldrich, St. Louis, MO) and 0.03% hydrogen peroxide in TBS for 10 min. Tissue

was then washed with TBS (3  $\times$  3 min), mounted on gelatin coated slides, and dried overnight. For Gal-3 stained tissue, slides were lightly counterstained in 0.5% thionin (pH 4.8) for 30 s. All slides were then dehydrated through graded alcohols (0, 50, 75, 95, 100, and 100%, 3 min each), and cleared in xylenes (2  $\times$  5 min). Slides were coverslipped with Permount (Fisher Scientific, Waltham, MA).

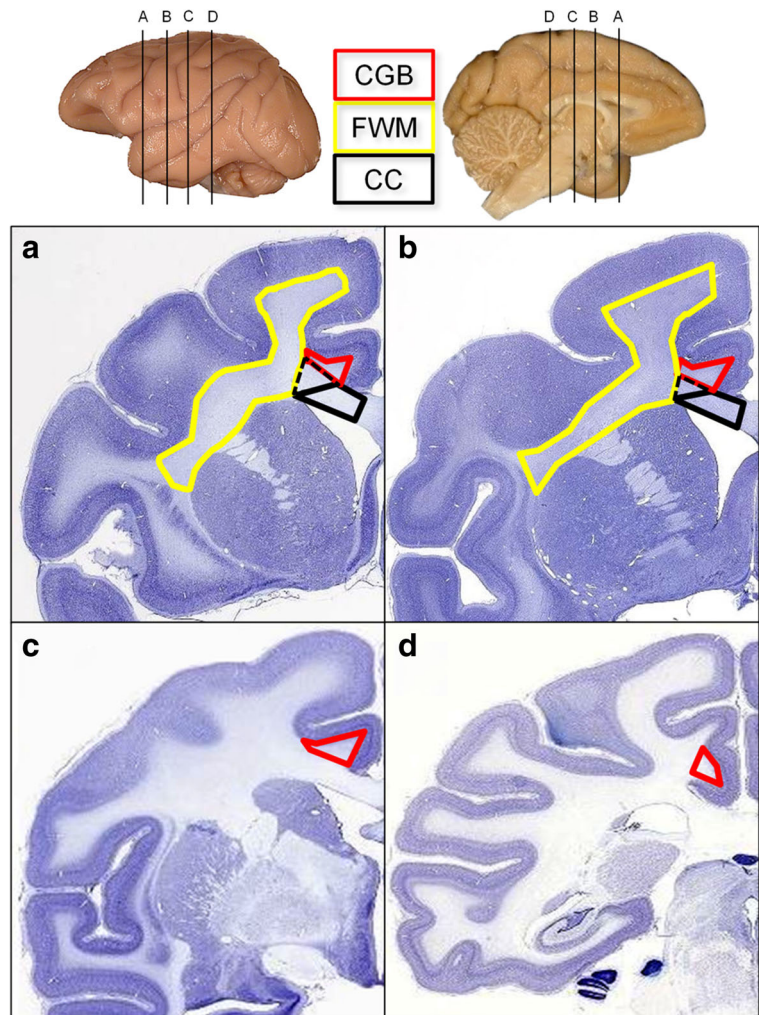
### Regions of interest

Regions of interest were identified using a  $\times 2$  objective, and boundaries were outlined according to the criteria illustrated in Fig. 2.

*Cingulum bundle* (Fig. 2a–d) The cingulum bundle (CGB) was defined as a semi-triangular white matter region within the cingulate gyrus. For the Gal-3 experiments and the rostral sections in the LN3 experiments, the CGB was bounded ventrally by the CC. The caudal portions of the CGB used in the LN3 experiments are bounded by the cingulate gyrus gray matter and an arbitrary line connecting area 29a–c to the junction of area 31 and the parietal area PE cingulate.

*Corpus callosum* (genu, Fig. 2a, b) For the genu of corpus callosum (CC), LN3 cell counting was bounded slightly more medially than that of Gal-3 counting; thus, the entirety of the CC defined in the LN3 experiment was contained in the CC defined in the Gal-3 experiment. For the LN3 experiment, the anterior edge of the CC was identified in the first serial section containing callosal fibers from the midline. For Gal-3 experiments, the most rostral section was identified as the first section containing both CC and internal capsule. The posterior end of the genu for both experiments was identified when the septum pellucidum first appears as it separates the anterior body from the rostrum. The dorsomedial boundary of the genu is the indusium griseum or the lateral ventricle (once the caudate is present), and the dorsolateral boundary is the anterior cingulate gyrus. For LN3 sampling, the lateral boundary of the genu is defined as a straight line connecting the medial edge of the gray/white boundary of the anterior cingulate to the lateral edge of the indusium griseum or the lateral edge of the lateral ventricle (once the caudate is present). For Gal-3 experiments, the lateral boundary of the CC extended from the lateral edge of the lateral ventricle to the ventrolateral edge of the cingulum bundle as to not overlap with the CGB or the FWM.

**Fig. 2** Nissl-stained sections from the NIH Blueprint NHP Atlas, (<http://www.blueprintnhatlas.org/static/home>) show the approximate rostral and caudal boundaries for each region of interest analyzed: the cingulum bundle (CGB, red), frontal white matter (FWM, yellow), and genu of the corpus callosum (CC, black). For the Gal-3 experiment, the CGB was sampled between AP+30.00 (a) and AP+25.50 (b), whereas for the LN3 experiment, the CGB was sampled between AP+17.45 (c) and AP+0.30 (d). For both Gal-3 and LN3 experiments, the FWM was analyzed from AP+30.00 (a) to AP+25.50 (b). For the LN3 analysis, cells in the CC were counted within the black solid boundary. For the Gal-3 experiment, the CC region of interest included the solid black line plus the region within the black dotted line. Interaural measurements estimated from Paxinos, Huang, & Toga (2000)



**Frontal white matter (Fig. 2a, b)** For both experiments, the frontal white matter (FWM) was defined as the white matter region excluding corpus callosum and cingulum bundle starting from the lateral most junction of the CC and caudate nucleus, ventral lateral across the putamen, then ventral to the intersection of the putamen and the claustrum and dorsal to the white matter beneath the inferior arcuate sulcus. The FWM then follows the border of the gray matter around to where it began.

#### Unbiased stereology

Standard unbiased stereology was performed on blind coded sections using a Nikon E600 light microscope equipped with a Q-Imaging digital camera, a motorized stage and Stereo Investigator software (MBF Bioscience, Williston, VT). Gal-3- and LN3-positive cells

were identified using the soma as the counting target and numbers estimated using the optical fractionator method as described by West et al. (1991). For each ROI and marker, pilot studies were performed to determine appropriately sized sampling grids and counting frames. For Gal-3-stained tissue, four to seven sections were used for each animal. Sections were blind coded and counted using a  $\times 20$  objective lens within a counting frame of  $99.0 \times 66.6 \times 10 \mu\text{m}^3$  with the dissector top guard volume extending  $5 \mu\text{m}$  below the tissue section surface. For LN3-stained tissue, six to ten sections were blind coded and counted using a  $\times 60$  oil-immersion objective lens within a counting frame of  $60 \times 60 \times 5 \mu\text{m}^3$  with the dissector top guard volume extending  $1 \mu\text{m}$  below the tissue section surface.

The sampling grid was randomly placed over the outlined ROI prior to counting. Cells were considered

to be Gal-3 or LN3 positive if they contained dark brown staining of a small cell body and at least one process or an enlarged circular cell body alone. The cell body was used as the counting object for cells that fell within the dissector or across its inclusion planes. The Cavalieri estimator was used to estimate volumes, and the coefficient of errors (CE) was calculated as described by Gundersen et al. (1999). With the counting frame and sampling grid used in the current study, a minimum of 100 cells for each region and animal and were counted and the CE was 0.1 or less to ensure minimal variance due to sampling. Due to the low number of Gal-3-positive cells in young and middle-aged animals, CE values below 0.1 were unattainable, making stereological estimations of total cell counts difficult. Therefore, cell density reported in cubic millimeters was used to compare relative counts between subjects.

### Morphology

In old animals (ages 20+), subtypes of Gal-3-positive cells were identified and counted according to the morphological criteria as ramified, hypertrophic, or amoeboid (see Fig. 3) as defined by Karperien et al. (2013). As shown in Fig. 3, cells were counted as ramified if they had one or more thin process extending from a small, dense cell body. Amoeboid cells were identified if they had enlarged, semi-circular cell bodies with limited to no processes extending from the soma. Hypertrophic cells were identified if they had any of the following: (1) a semi-circular or rod-like cell body with no processes; (2) an enlarged, non-circular cell body with at least one process; or (3) an enlarged, non-circular cell body with dark, dense, and thicker processes.

### Immunofluorescence colocalization and quantification

For double-label immunofluorescence of activated microglia (LN3+) and the phagocytic phenotype (Gal-3+), two sections containing FWM from each of 19 animals were stained using mouse IgG2b anti-LN3 and mouse IgG1 anti-Gal-3. Sections were thawed together and first washed with buffer to remove the glycerol and then incubated in SuperBlock for 1 h, and placed in 0.5% SuperBlock, 0.3% Triton-X solution containing LN3 (1:62.5), and Gal-3 (1:150) overnight at room temperature. As negative controls, sections were either incubated in carrier solution, carrier solution containing Gal-3, or

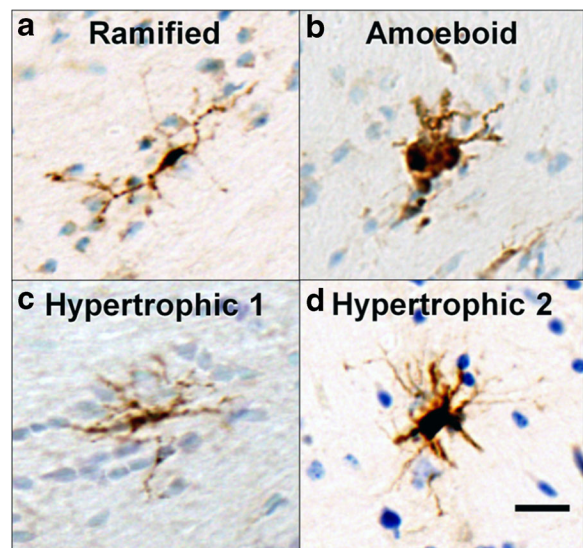


**Fig. 3** Morphological characterization of Gal-3-positive cells. Ramified microglia (**a**) contain dense cell bodies and thin processes distributed around the cell. Amoeboid microglia (**b**) are characterized by large, round stained cells with only a few, short processes or no processes. As shown in **c** and **d**, hypertrophic Gal-3-positive cells are found in a variety of shapes and sizes but range from cells with an elongated cell body and short, dense processes (Hypertrophic 1; **c**) to cells with a densely stained and curved cell body with short, dense processes or intense cell body staining with thin processes extending outwards (Hypertrophic 2; **d**). Scale bar = 20  $\mu$ m

carrier solution containing LN3. Following primary antibody incubation, tissue was washed with TBS then incubated in secondary antibody solution containing 0.5% SuperBlock, 0.3% Triton X, AlexaFluor 488 goat anti-mouse IgG2b (1:1000, Invitrogen, Carlsbad, CA), and AlexaFluor 568 goat anti-mouse IgG1a (1:1000, Invitrogen, Carlsbad, CA). Sections were then washed and mounted. Once semi-dry, the slides were rehydrated in buffer for 5 min, then dehydrated in 70% ethanol for 5 min and incubated with Autofluorescence Eliminator Reagent (Millipore, Darmstadt, Germany) for 45 s. The slides were cleared with 70% ethanol ( $3 \times 1$  min) and coverslipped using anti-fading mounting medium (PVA-DABCO, Sigma-Aldrich, St. Louis, MO).

Colocalization of Gal-3 and LN3 was determined in the FWM of young and old animals using a Leica TCS SPE laser scanning confocal microscope (Buffalo Grove, IL). AlexaFluor-488 emission was detected using argon laser excitation at 488 nm whereas Alexafluor-568 emission was detected using 561-nm laser excitation. To ensure equal counting between animals, exhaustive searches were first performed for the less dense Gal-3-



labeled cells in young animals. Prescanning determined that 25 z-stack images could be taken per animal with at least 1 Gal-3-positive cell per image identified with a  $\times 40$  objective lens. The width of the image was determined by the point where no Gal-3-positive staining was visualized. The number of z-slices was determined using the automated system optimized settings. LN3 was visualized in green and Gal-3 in magenta. Cells in each image were counted as single-labeled Gal-3 (magenta only in a cell body with at least one process) or double-labeled Gal-3 with LN3 (white image of double-labeled cell body with at least one process). Double-labeled cells were further subdivided into two categories: (1) overlapping double label (white staining verified as double labeling by investigation of individual color channels) and balloon double label (magenta “ballooned” white or magenta process extending from a cell body encircled by green label).

Z-stack images contained in .LIF files were counted using FIJI (version 1.49m, National Institutes of Health). Individual channels for green and magenta were opened, and contrast was automatically enhanced. The channels were then merged and the z-stack compressed using the z-projection function to flatten all images in the stack to one image. The percentage of each type of Gal-3 labeling was determined by manual counting with the investigator blind to subject conditions.

### Statistics

All analyses were performed using the R-project ( $\times 64$ , version 3.10) and RStudio (version 0.98.1102) for statistical computing and an alpha significance level of 0.05. Three-factor ANOVA with two between-subject factors (age groups (3)  $\times$  sex (2)) and one repeated measure (region (3)) was performed with subjects stratified by young, middle-age, and old. When statistically significant differences were found by ANOVA, a Tukey-A (HSD) post hoc test was used to identify the critical factor while controlling for multiple comparisons. Linear regression analyses ( $\alpha = 0.05$ ) were conducted to assess the relationship of LN3 cell density, Gal-3 cell density, and Gal-3 morphological subtype density to age or cognitive function (in old animals only). A chi-squared test of independence was used to test differences in Gal-3 double labeling with LN3 between young and old animals.

## Results

### Galectin-3 phagocytic cell density increases with age

Examples of Gal-3 staining are shown in Fig. 4a, b, and the volume of each ROI and the estimated Gal-3-positive cell density is shown in Table 2 for each animal. To determine if the density Gal-3-positive staining (cells/mm<sup>3</sup>) differed by sex or ROI, animals were stratified into age groups (young, middle-aged, old) and ANOVA was used to assess the effects of age group, sex, and ROI. There were no significant differences in density of Gal-3-positive cells between regions ( $F(2,64) = 0.085$ ,  $p = 0.919$ ) or between sexes ( $F(1,64) = 0.026$ ,  $p = 0.873$ ), but Gal-3 cell density did approach significance by age ( $F(2,64) = 2.763$ ,  $p = 0.071$ , see Fig. 5a) and there were no significant interaction effects between factors. A Tukey-A post hoc analysis was performed comparing Gal-3 cell densities across sex, ROIs, and groups. This post hoc analysis demonstrated that the density of Gal-3+ cells was significantly higher in old animals compared to both young ( $p \leq 0.00001$ ) and middle-aged animals ( $p \leq 0.00001$ ). Middle-aged animals did not significantly differ from young animals ( $p = 0.243$ ). These differences were consistent for all ROIs.

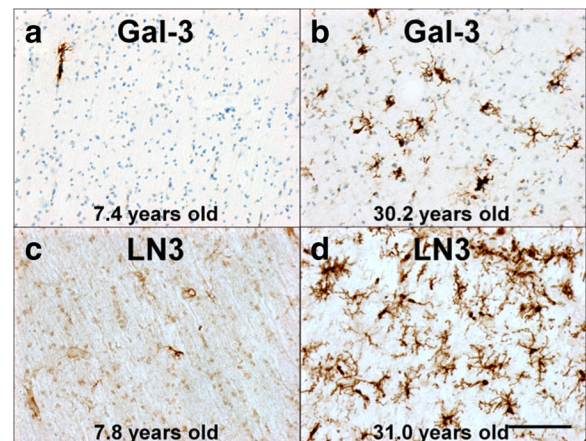


**Fig. 4** These photomicrographs compare typical staining in the frontal white matter for Gal-3- and LN3-positive cells. **a** Scarcity of Gal-3 staining in a young subject (AM222) compared to the robust staining in **b** for an aged subject (AM121). Similarly, **c** shows sparse LN3-positive staining in a young subject (AM198) compared to dense staining in **d** for an aged subject (AM119). A thionin counterstain was used for Gal-3-stained sections, as indicated by blue staining seen in **a** and **b**. Scale bar = 0.1 mm

**Table 2** Galectin-3 experiment: cell density and volume for each subject

Subject	Age	Sex	Group	CII	Galectin-3 cell density(cells/mm <sup>3</sup> )			Volume (mm <sup>3</sup> )		
					CC	CGB	FWM	CC	CGB	FWM
AM204	6.1	M	Y	-0.82	NA	104	NA	NA	30	NA
AM188	6.5	F	Y	0.36	32	69	560	57	42	564
AM299	7.1	F	Y	0.85	360	NA	179	56	NA	486
AM222	7.4	M	Y	0.87	404	201	337	89	49	629
AM296	8.7	M	Y	0.77	313	219	231	69	29	418
AM255	9.5	F	Y	0.12	119	72	53	72	29	411
Young	Average (std dev)				246 (162)	133(72)	272 (191)	69 (13)	37 (10)	502 (94)
AM214	10.7	F	MA	1.2	NA	NA	363	NA	NA	366
AM295	10.8	M	MA	1.52	98	50	155	66	27	638
AM194	11.9	F	MA	2.26	310	438	557	61	27	614
AM195	12.1	F	MA	0.03	529	874	572	70	28	828
AM291	13.7	F	MA	1.17	58	111	89	76	24	581
AM278	15.3	F	MA	2.68	303	819	222	49	29	693
AM215	16.6	M	MA	3.89	333	220	234	46	16	616
AM257	17.6	F	MA	1.56	856	726	492	33	19	453
AM190	18.0	F	MA	1.53	561	709	431	50	22	591
AM250	18.0	F	MA	6.01	683	644	679	61	23	578
AM274	18.3	F	MA	2.28	777	759	438	62	28	727
Middle-aged	Average (std dev)				451 (274)	535 (307)	385 (189)	57 (13)	24 (4)	608 (125)
AM256	20.7	F	O	1.93	2498	2322	1500	86	30	699
AM200	21.0	F	O	4.14	689	365	408	50	24	399
AM286	22.4	F	O	1.43	NA	624	293	NA	12	247
AM208	22.7	M	O	1.09	3166	NA	1541	138	NA	760
AM282	23.0	M	O	4.20	1928	2230	857	62	34	347
AM179	23.6	F	O	6.99	432	510	420	57	26	514
AM284	25.4	M	O	1.47	1185	1406	638	76	35	675
AM220	25.7	F	O	8.77	4776	3427	3010	64	27	483
AM110	25.8	M	O	7.93	1363	1683	1436	77	38	799
AM298	26.7	M	O	1.28	1952	1370	811	52	55	1195
AM275	27.8	F	O	1.60	1702	1723	841	54	33	546
AM104	28.9	F	O	2.15	1513	1508	984	81	24	664
AM180	29.6	F	O	3.51	1739	1670	1288	52	21	365
AM121	30.2	M	O	12.37	1088	1286	3131	67	41	511
Old	Average (std dev)				1849 (1136)	1548 (822)	1226 (881)	70 (24)	31 (11)	586 (241)

To test the hypothesis that Gal-3 cell density increased with age, linear regression was used with age as a continuous variable. There was a significant age-related increase in the density of Gal-3-positive cells in the CGB (Fig. 5b, ( $F(1,26) = 29.9, p \leq 0.0001$ ) with age accounting for approximately 51.7% of the variance in Gal-3 cell density ( $R^2 = 0.517$ ). Similarly in the FWM

(Fig. 5c), the density of Gal-3-positive cells significantly increased with age ( $F(1,27) = 31.6, p \leq 0.0005$ ) which accounted for 52.2% of the variance in Gal-3 cell density ( $R^2 = 0.522$ ). Similarly, in the CC (Fig. 5d), Gal-3 cell density significantly increased with age ( $F(1,26) = 17.3, p \leq 0.0005$ ) where it accounted for 37.6% of the variance.

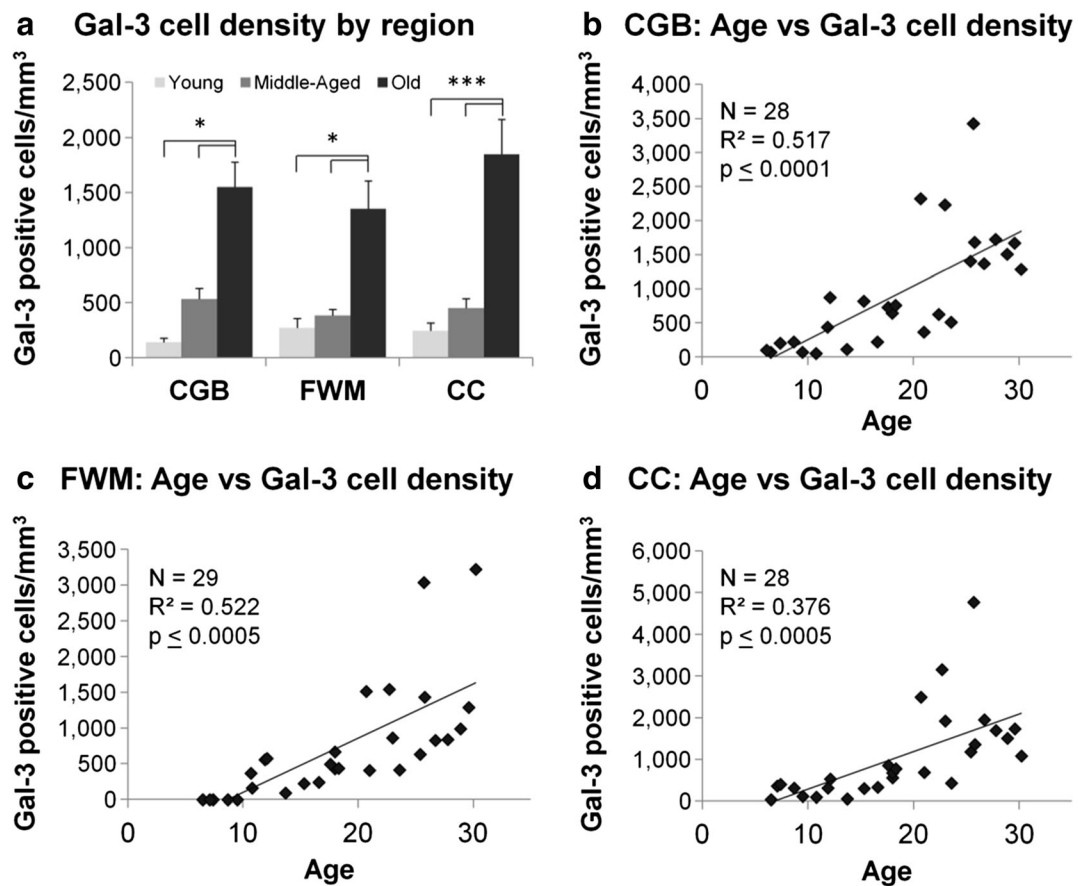


**Fig. 5** a Bar graphs comparing Gal-3 cell density for each region stratified by age groups. A three-way ANOVA demonstrated that while there were no significant effects of sex or regions, there was a significant effect of age groups. Tukey-A post hoc analysis demonstrated that within each region of interest, Gal-3 cell density

was significantly greater in old animals compared to young and middle-aged animals. Scatterplots of Gal-3 cell density in each region of interest are shown in **b–d**. Linear regression analysis showed that Gal-3 cell density was positively associated with age in all three regions. \* $p \leq 0.05$ , \*\*\* $p \leq 0.0005$

LN3-activated microglial density increases regionally with age

LN3-positive staining can be seen in Fig. 4c, d. To determine if there were statistical differences between LN3 cell density (cells/mm<sup>3</sup>), a three-way ANOVA was run with subjects stratified by age, sex, and ROI (Table 3). There was no significant effect of sex ( $F(1,35) = 0.53$ ,  $p = 0.473$ ), but there were significant effects for region ( $F(2,35) = 7.72$ ,  $p \leq 0.005$ ) and age group ( $F(2,35) = 3.97$ ,  $p \leq 0.05$ ). There were no significant interaction effects. To further investigate the significant differences in age groups, one-way ANOVA analyses were performed between cell density and age group for each of the three regions. There were no significant differences in LN3 cell density between age groups in the CC ( $F(2,15) = 1.42$ ,  $p = 0.272$ ) or in the

FWM ( $F(2,15) = 2.56$ ,  $p = 0.111$ ). However, LN3 cell density did differ significantly by group in the CGB ( $F(2,15) = 7.70$ ,  $p \leq 0.005$ ). Tukey post hoc analysis revealed that old animals had significantly greater LN3-positive cell density compared to both middle-aged ( $p \leq 0.05$ ) and young animals ( $p \leq 0.01$ , see Fig. 6a,d

Linear regression analysis was used to determine if density of LN3-positive cells in each region was associated with age. As shown in Fig. 6b, the density of LN3-positive cells in the CGB significantly increased with age ( $F(1,16) = 22.1$ ,  $p \leq 0.0005$ ), where age accounted for 54.0% of the variance in LN3 cell density ( $R^2 = 0.540$ ). In the FWM (Fig. 6c), the relationship between age and LN3 cell density approached significance ( $F(1,16) = 4.12$ ,  $p = 0.059$ ) and age explained 15.5% of the variance in LN3-positive cell density ( $R^2 = 0.155$ ). In the CC (Fig. 6d),

**Table 3** LN3 experiment: cell density and volume for each subject

Subject	Age	Sex	Group	LN3 cell density (cells/mm <sup>3</sup> )				Volume (mm <sup>3</sup> )			
				CII	CC	CGB	FWM	CC	CGB	FWM	
AM188	6.5	F	Y	0.36	2302	5647	NA	36	119	NA	
AM132	7.5	M	Y	0.35	4133	4088	23,163	35	164	483	
AM093	7.6	M	Y	-0.09	4316	3338	10,398	34	145	369	
AM128	7.9	M	Y	2.89	2021	1758	22,030	25	111	501	
AM198	7.8	F	Y	-0.95	490	2340	8461	29	143	546	
Young				Average (std dev)		2652 (1593)	3434 (1528)	16,013 (7657)	32 (5)	136 (21)	475 (75)
AM066	11.2	F	MA	0.79	575	826	4734	32	88	536	
AM194	11.9	F	MA	2.26	2850	2910	10,965	26	129	490	
AM138	12.1	M	MA	NA	225	743	5765	35	145	482	
AM190	18.0	F	MA	1.53	4084	7481	18,995	31	139	390	
AM153	19.5	M	MA	1.00	6838	8476	22,929	41	140	432	
AM125	19.8	F	MA	3.13	2111	6323	20,087	24	104	335	
AM124	19.9	M	MA	0.94	931	6296	19,365	37	145	529	
Middle-aged				Average (std dev)		2516 (2343)	4722 (3190)	14,691 (7417)	32 (6)	127 (22)	456 (74)
AM189	24.5	M	O	2.90	2558	8398	13,154	32	141	491	
AM064	24.9	M	O	0.43	4877	9400	38,911	34	125	400	
AM090	25.0	F	O	1.03	4991	11,263	52,961	27	97	287	
AM104	29.0	F	O	2.15	6080	5328	15,673	27	104	384	
AM180	29.6	F	O	3.51	5580	10,281	27,221	24	104	368	
AM121	30.2	M	O	12.37	940	5543	17,888	33	123	459	
AM119	31.0	F	O	2.69	4806	11,413	22,625	36	149	389	
Old				Average (std dev)		4262 (1834)	8804 (955)	26,919 (14,364)	30 (4)	120 (20)	397 (66)

the relationship between LN3 cell density and age again approached significance ( $F(1,17) = 3.70$ ,  $p = 0.072$ ) but age accounted for only 13.0% of the variance in LN3-positive cell density ( $R^2 = 0.13$ ).

Gal-3 cells are a subset of LN3-positive microglia

To determine if Gal-3-positive phagocytic cells also expressed the “activated” LN3 phenotype, the percentage of Gal-3 cells double-labeled with LN3 was determined in young and old animals using immunofluorescence and confocal microscopy. As shown in Fig. 7a–c, two different classes of cells were identified: (1) single-labeled, a cell that was Gal-3-positive and LN3-negative, and (2) double-labeled, a cell that contained both Gal-3 staining and LN3 staining.

Additionally, as shown in Fig. 7e, some of the double-labeled cells had a distinct morphology with the Gal-3 signal contained within an LN3-positive “balloon” within the LN3-positive cell, but without necessarily overlap of both labels. For all subjects, 91.3% of Gal-3-positive cells were double-labeled with LN3 and only 8.7% were not. Additionally, of the Gal-3-positive cells, 75.5% of Gal-3 staining showed almost complete overlap with LN3 whereas 15.8% of cells the Gal-3-positive signal was surrounded by an LN3 balloon (Fig. 7d). To determine if the proportion of Gal-3 double-labeled with LN3 differed between ages, a chi-squared test was performed and revealed no significant differences between young and old animals ( $\chi^2(1, N = 20) = 0.767$ ,  $p = 0.678$ ).

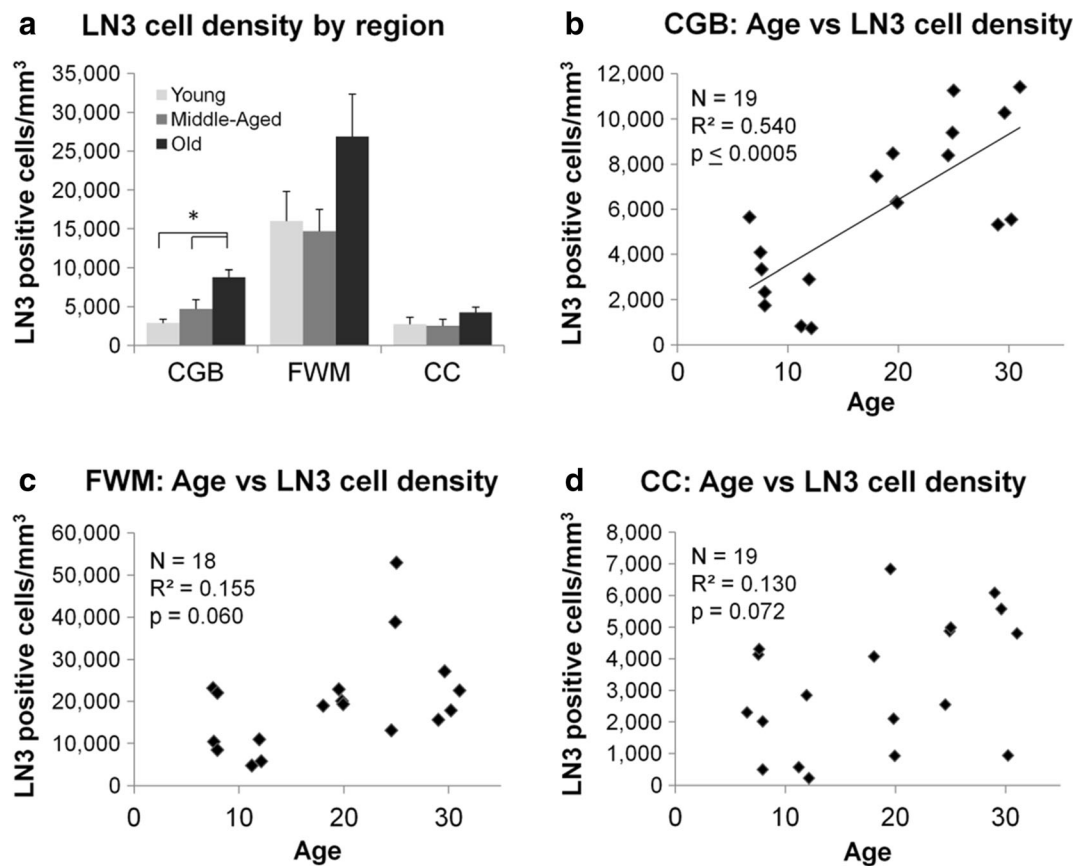


**Fig. 6** a Bar graphs displaying LN3 cell density for each region stratified by age group within each region of interest. A three-way ANOVA demonstrated that there was no significant effect of sex, but there were significant effects of age groups ( $p \leq 0.05$ ) and within regions ( $p \leq 0.005$ ) with no significant interactions. Tukey-A post hoc analysis demonstrated that within the CGB, LN3 cell

density was significantly greater in aged subjects compared to middle-aged ( $p \leq 0.05$ ) and young ( $p \leq 0.01$ ). Scatterplots of LN3 cell density in each region of interest are shown in **b–d**. Linear regression analysis demonstrated that LN3 cell density was positively associated with age in the CGB and approached a statistical association in the FWM and the CC. \* $p \leq 0.05$

#### Density of hypertrophic and amoeboid Gal-3 cells predicts cognitive decline

To determine if microglial activation or phagocytic phenotype were associated with age-related cognitive impairment, linear regression was used to compare density to CII score of old animals (ages 20+ years) with each marker. CII was not associated with LN3 cell density in the CGB ( $F(1,4) = 0.007$ ,  $p = 0.937$ ,  $R^2 = 0.248$ ) or the FWM ( $F(1,5) = 1.24$ ,  $p = 0.317$ ,  $R^2 = 0.038$ , Fig. 8a) but was significantly predicted by LN3 cell density in the CC ( $F(1,4) = 8.37$ ,  $p \leq 0.05$ ,  $R^2 = 0.551$ ). However, this effect was largely driven by one animal (AM121). Using a multiple of 1.5 times the interquartile range, AM121 was identified as an outlier for CII score. When

AM121 was removed, the CII score was no longer predicted by LN3 cell density in the CC ( $F(1,4) = 0.07$ ,  $p = 0.799$ ,  $R^2 = 0.227$ ).

For Gal-3, there was no relationship between cell density and CII in the CGB ( $F(1,11) = 0.27$ ,  $p = 0.614$ ,  $R^2 = 0.065$ ) or the CC ( $F(1,11) = 0.010$ ,  $p = 0.923$ ,  $R^2 = 0.09$ ). However, increased Gal-3 cell density in the FWM significantly predicted increased CII ( $F(1,12) = 10.8$ ,  $p \leq 0.01$ ) accounting for 42.9% of the variance in CII score ( $R^2 = 0.429$ ).

To determine if the significant relationship of Gal-3 cell density in the FWM to CII score was due to phagocytic morphologies, linear regression was used to assess the relationship between the densities of ramified, hypertrophic, and amoeboid Gal-3-positive cells and CII of animals 20 years or older. While the density of ramified Gal-3 cells was

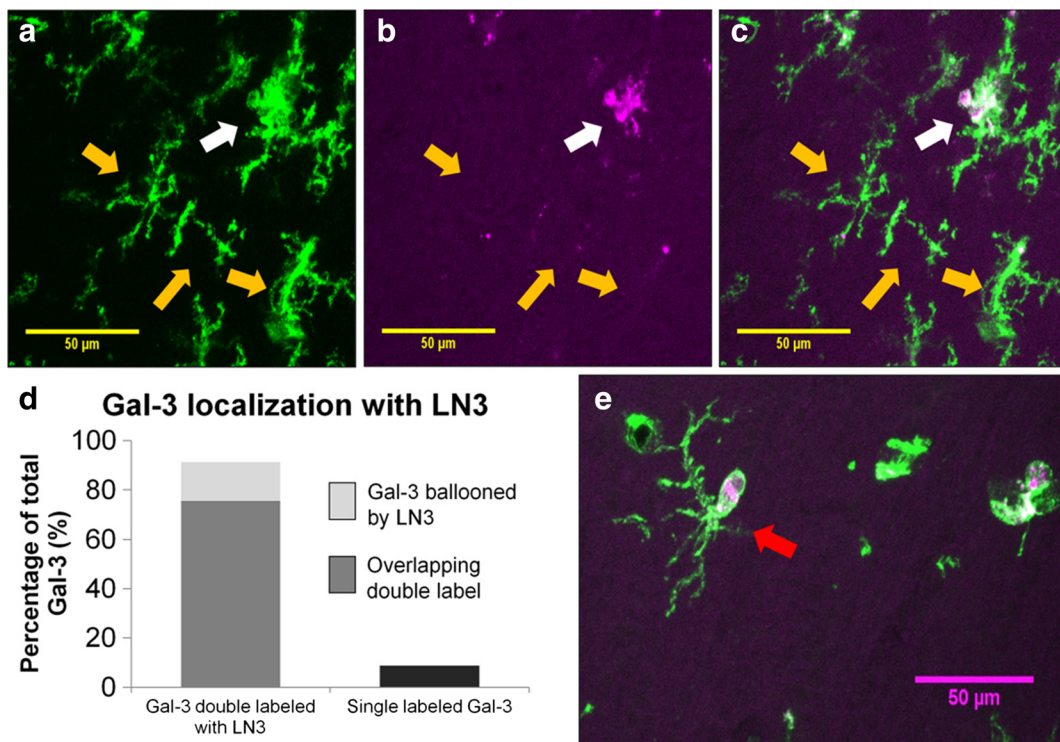


**Fig. 7** Confocal images were taken in a z-stack and compressed into single layers using FIJI software. Examples of this compression are shown in **A** for LN3 only (*green*) and in **B** for Gal-3 only (*magenta*). **c** Merged image and shows one cell with colocalization in white (*white arrow*) while the other three cells indicated by *yellow arrows* remain single-labeled for LN3. **d** Gal-3 is found in

91.3% of LN3-positive cells while 8.7% of Gal-3 cells do not colabel with LN3-positive cells. As shown in **e**, a subset of the Gal-3 and LN3<sup>+</sup> double-labeled cells contained small, round, offshoots of LN3 that surrounded, but did not always colocalize with Gal-3 staining. These offshoots are referred to as “balloons” and one is indicated by the *red arrow*. Scale bars = 50  $\mu$ m

not associated with CII ( $F(1,11) = 0.98$ ,  $p = 0.343$ ,  $R^2 = 0.002$ , Fig. 8b), CII was significantly predicted by the density of amoeboid Gal-3 cells ( $F(1,10) = 16.94$ ,  $p \leq 0.005$ ,  $R^2 = 0.592$ , Fig. 8c) and also by the density of hypertrophic Gal-3 cells ( $F(1,11) = 0.05$ ,  $p \leq 0.05$ ,  $R^2 = 0.357$ , Fig. 8d).

## Discussion

### Summary

The current study utilized immunohistochemical labeling with Gal-3 and LN3 antibodies to identify phagocytic and activated microglial in the brains of cognitively assessed rhesus monkeys. In the cingulum bundle, corpus callosum, and frontal white matter, Gal-3 and LN3 cell densities increased significantly with increasing age. Of the Gal-3<sup>+</sup> phagocytic microglia, 90%

colocalized with LN3 marker for activated microglia. In about 15% of the Gal-3-positive cells, the markers were not fully overlapped but, instead, showed a small Gal-3-positive outgrowth characterized as Gal-3<sup>+</sup> phagocytic “balloons.” While total numbers of double labeling and Gal-3 balloons increased with age, the percentage of double-labeled Gal-3 and ballooned Gal-3 did not differ between age groups. To determine if either phagocytic activation or total microglial activation were related to the degree of age-related cognitive decline, the densities of Gal-3<sup>+</sup> and LN3<sup>+</sup> microglia were evaluated in behaviorally tested old monkeys ( $\geq 20$  years of age). In these aged subjects, increased Gal-3<sup>+</sup> cell density correlated with increased cognitive decline in the frontal white matter but not in the cingulum or the genu of the corpus callosum. In contrast, LN3<sup>+</sup> cell density only correlated with cognitive performance in the corpus callosum although this was mainly driven by one animal that was very impaired. Since

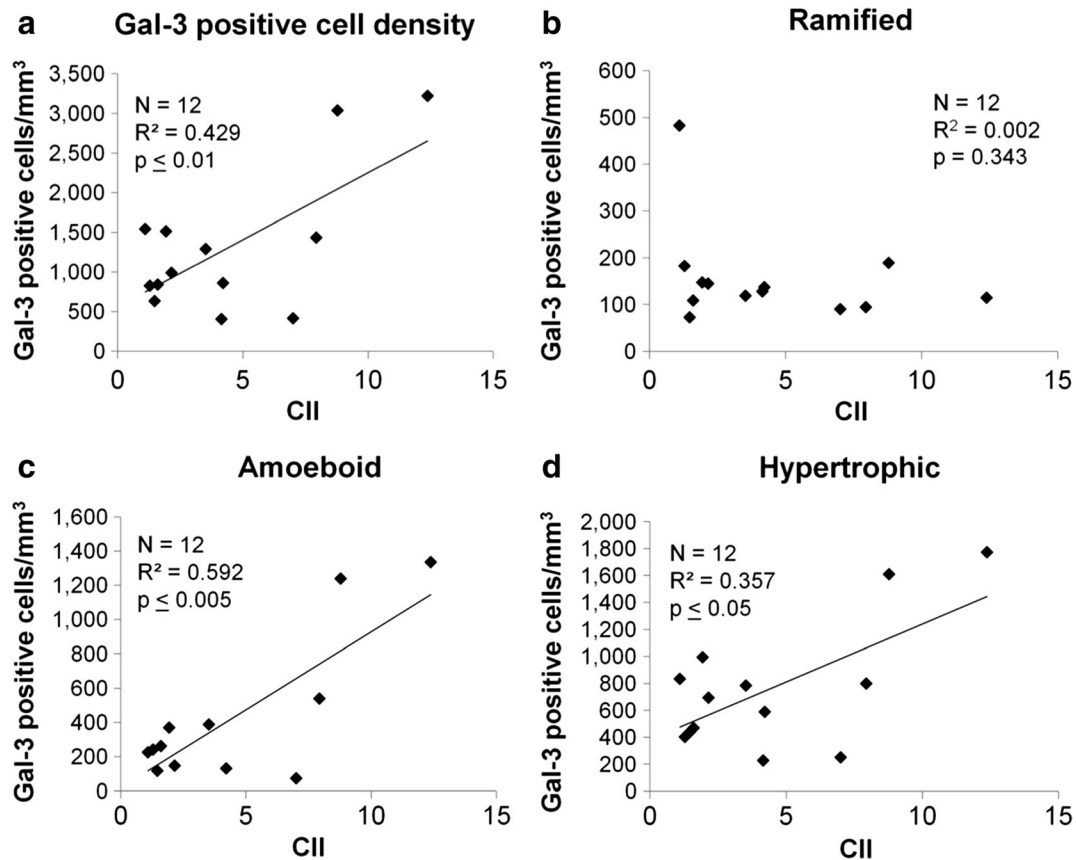


**Fig. 8** Scatterplots showing the relationship of cognitive impairment (CII) to Gal-3-positive cell density in total and by morphological subtypes in the FWM of old animals (ages 20+). Regression analysis showed that CII is significantly related to **a** total Gal-3 cell density, but not **b** to the density of ramified Gal-3 cells.

However, the density of **c** amoeboid Gal-3 cells and **d** hypertrophic Gal-3 cells both significantly predicted by CII score. This suggests that only the inflammatory-associated amoeboid and hypertrophic morphologies of Gal-3 cells are associated with increased cognitive impairment

microglial morphology may be indicative of function (Karperien et al. 2013), we analyzed morphological subtypes of Gal-3+ cells in the frontal white matter of the aged animals to determine if the previously identified correlation of Gal-3+ cell density and cognitive impairment was due to microglia with an activated morphology. While the density of Gal-3+ cells with a ramified morphology was not related to cognitive impairment, the density of both hypertrophic and amoeboid subtypes was significantly associated with increased cognitive impairment.

#### Functional classification of microglia by immunohistochemistry and morphology

Microglia have been dichotomized as M1/pro-inflammatory which corresponds with the classical notion of activation or as M2/anti-inflammatory which is

an alternative activation state. In vitro, M1 activation is defined by responsiveness to IFN- $\gamma$  or LPS challenge causing release of pro-inflammatory cytokines such as TNF- $\alpha$  or IL-6, and production of reactive oxygen species. The alternative M2 activation is defined by responsiveness to IL-4 leading to the release of anti-inflammatory cytokines such as TGF- $\beta$  and IL-10 (for review on microglia activation, see Cherry et al. 2014). However, identifying, defining, and interpreting activation states in vivo has been inconsistent (Gordon and Martinez 2010; Prinz and Priller 2014). For example, the current study utilizes LN3, an antibody to the HLA-DR MHC II surface receptor as a marker for microglial activation. Some report that MHC II expression increases with microglial “activation” following pathogen-associated molecular patterns (Town et al. 2005). However, MHC II expression is regulated by toll-like receptor stimulation and the M1 activation

pathway via IFN- $\gamma$  (Ting and Trowsdale 2002) but nevertheless is associated with both pro- and anti-inflammatory phenotypes (Conde and Streit 2006). Hence, MHC II expression can also be regarded as a marker for identifying the general population of microglial (Conde and Streit 2006; Mittelbronn et al. 2001). While the Gal-3 literature is more consistent in that it is necessary for phagocytosis (Sano et al. 2003; Dumic et al. 2006), Gal-3 has not been widely utilized in the brain and only recently recognized as a marker for phagocytic activation (Safaiyan et al. 2016).

Thus, immunohistochemical staining with LN3 or Gal-3 may not necessarily indicate the presence of a specific functional state (activation or phagocytosis). Rather Gal-3+ staining may simply indicate that the microglial cell is “primed” for phagocytic activation while the presence of LN3+ staining may indicate the cell is “primed” for inflammatory activation (Norden and Godbout 2013; Perry and Holmes 2014). Double labeling with LN3 and Gal-3 would indicate that both processes are available when necessary. Consistent with this interpretation of microglia priming, Sierra et al. (2007) showed that while aged mice have higher baseline mRNA expression of both M1 cytokines (TNF- $\alpha$ , IL-6, IL-1 $\beta$ ) and M2 cytokines (IL-10, TGF- $\beta$ ), when challenged with LPS, older mice have both more robust pro- and anti-inflammatory cytokine responses compared to young mice. This indicates that microglia that appear as “activated” by IHC may be primed and ready to respond when challenged. Therefore, the current data demonstrate that both phagocytic priming (Gal-3+ cells) and general microglial activation increase with age in frontal white matter regions. Further, as over 90% of Gal-3 cells are colabeled with LN3, it is clear that the majority of phagocytic primed cells are activated microglia.

Further insight into functional state may be gained by examining the morphological subtypes of labeled microglia. As reviewed by Karperien et al. (2013), ramified microglia with small, round cell bodies and thin processes are thought to be non-inflammatory, surveilling the neuronal environment for damage (Nimmerjahn et al. 2005). In contrast, hypertrophic microglia are often polarized, with enlarged soma and denser processes representative of “activated” or inflammatory microglia (Lee et al. 2008). Amoeboid microglia with rounded somata and limited processes are indicative of phagocytic microglia (Bohatschek et al. 2001). Although these data suggest that

morphology is indicative of function, no study to date has demonstrated exactly what cytokines are being released or what exact functions are occurring in each morphological state. Hence, the traditional M1/M2 dichotomy and division into “activated” and “resting” cells is being re-examined (Ransohoff 2016). In the current study, phagocytic microglia stained for Gal-3 are separated by these morphological subtypes. As expected, the Gal-3-positive cells were primarily hypertrophic or amoeboid. Moreover, only the density of hypertrophic and amoeboid Gal-3+ cells correlated with cognitive impairment. The observation that ramified Gal-3+ cells do not change with age or predict cognitive decline suggests that there is a baseline number of Gal-3+ cells that are primed for phagocytosis but have not developed an inflammatory phenotype. The changes in total Gal-3+ staining likely indicates an increase in the number of cells taking on morphologies indicative of an inflammatory phenotype. This demonstrates that Gal-3 immunoreactivity is a useful marker for inflammation and phagocytosis in the brain.

#### Microglial activation and phagocytosis throughout the lifespan

One hallmark of brain aging is chronic M1/pro-inflammatory activation of microglia (Cribbs et al. 2012; Holtman et al. 2015, see Norden and Godbout 2013 for review). Increased overall microglial activation with age has been reported using different IHC markers in rodents (Rozovsky et al. 1998; Sierra et al. 2007), monkeys (Sheffield and Berman 1998; Sloane et al. 1999), and humans (DiPatre and Gelman 1997; Rogers et al. 1988; Streit and Sparks 1997). The current study confirms and expands upon this general finding by demonstrating that the density of LN3 (total activation) and Gal-3 (phagocytic activation) positive microglial increases with age in white matter pathways of the frontal lobe (the cingulum bundle, corpus callosum, and frontal white matter). Bowley et al. (2010) and many others (Feldman and Peters 1998; Peters and Sethares 2002; Sandell and Peters 2003) have reported an age-related accumulation of myelin defects and axon loss in forebrain white matter pathways of the rhesus monkey (e.g., the corpus callosum and cingulum bundle, anterior commissure). Additionally, others have shown age-related loss of white matter volume in MRI (Guttman et al. 1998; Wisco et al. 2008), increases in white matter hyperintensities in MRI (Tullberg et al. 2004;



Wakefield et al. 2010) and increased myelin damage inferred by loss of fractional anisotropy from diffusion tensor imaging (DTI; Makris et al. 2007). As myelin defects accumulate with age, it is likely that microglia would be activated and participate in the clearance of damaged white matter and axons. Interestingly, neither LN3 nor Gal-3 antibodies show robust staining in the gray matter in young or old monkeys (data not shown).

### Phagocytosis and demyelination

Despite the large body of evidence that myelin is damaged and lost and microglia are activated with age, evidence of myelin removal has been limited. Peters and Sethares (2002), using electron microscopy, described small myelin fragments in astrocytes and less frequently in microglia. This is in contrast to *in vitro* studies that report macrophages, such as microglia, phagocytose myelin at a greater rate than astrocytes (Williams et al. 1994). Other studies report that myelin phagocytosis is impaired with age (Ruckh et al. 2012; Natrajan et al. 2015) and can be inhibited by pro-inflammatory cytokines (Brück et al. 1992; Liu et al. 2006). Thus, it is possible that the chronically pro-inflammatory microglia of the aging brain could slow the removal and phagocytosis of myelin debris (Rawji et al. 2016).

In a demyelinating model of experimental autoimmune encephalomyelitis (EAE), Gal-3 expression has been shown to increase (Reichert and Rotshenker 1999), but, despite this increase, myelin clearance in this model is insufficient to allow recovery of myelination to normal levels (Neumann et al. 2009). Similarly, studies have shown that if myelin debris is not removed, remyelination is impaired (Lampron et al. 2015). In this regard, it is also known that oligodendrocyte precursor cells are recruited to areas of demyelination, but differentiation into mature myelinating oligodendrocytes is impaired by myelin debris (Kotter et al. 2005; Kotter et al. 2006). These observations suggest that a limiting factor in repair and restoration of myelin may be the phagocytic capacity of the microglia to remove myelin debris.

### Phagocytic functionality

The data from the current study, that Gal-3-positive cell density increases with age, suggest that stimulation of phagocytosis increases with age in parallel with myelin

damage. The correlation of increased phagocytic phenotype (amoeboid cells) with increased cognitive decline reported here and the age-related increase in myelin damage reported in this same model (see Peters and Kemper 2012 for review) likely means that phagocytosis is not sufficient to effectively remove damaged myelin (Ruckh et al. 2012; Natrajan et al. 2015). Hence, the observed increase in Gal-3-positive microglia with age could indicate that microglia have been “primed” for phagocytosis by detection of deteriorating myelin, but are either dysfunctional or the amount/rate of myelin damage is too much for microglia to efficiently phagocytose the debris. As more myelin debris accumulates and is not repaired, a vicious cycle could result in which more microglia are recruited and release pro-inflammatory cytokines, but fail to remove sufficient myelin debris to allow for remyelination and resolution of inflammation (Ruckh et al. 2012; Natrajan et al. 2015).

In our immunofluorescence study of Gal-3 colocalization with LN3, approximately 15% of the cells had a distinct balloon-like formation extending from an otherwise normal looking LN3+ microglial soma. This feature resembles the phagocytic cups previously described *in vitro* (Kay et al. 2006; Leverrier and Ridley 2001; Murray et al. 2005). These actin-dependent cups form during the initial stages of phagocytosis as a macrophage begins to engulf debris. It would be expected that the percentage of microglia displaying these phagocytic cups would increase with accumulating damage. To the extent that presence of Gal-3+ phagocytic balloons are markers of phagocytic function, the present data showed no difference in the percentage of cells double-labeled cells with phagocytic cups between young and old animals. Since all evidence suggests that white matter in the aged brain likely contains significant myelin damage, the lack of an increase in the percentage of microglia with phagocytic cup suggests an impairment in phagocytic responsiveness.

### Phagocytic capacity and age-related neurodegenerative diseases

With age, microglia have been described as dystrophic and senescent (Streit et al. 2004), but the functionality and phagocytic capacity of these senescent microglia is unknown. In a recent study in mice, Safaiyan et al. (2016) identified an age-related increase in Gal-3 microglia and an increase in microglia contacting myelin visualized by double-label IHC, suggesting that

microglia not only have increased phagocytic activation but also that this increased activation may be related to myelin. Similar inefficient debris clearance has been seen in age-related neurodegenerative diseases such as Alzheimer's, where  $\beta$ -amyloid aggregation is also thought to be related to an impaired phagocytic capacity of microglia (Chung et al. 1999; Lucin et al. 2013; Hickman and El Khoury 2014). These data suggest that age-related impairment of microglial phagocytosis is not limited to myelin. However, the question still remains as to the cause of the impaired microglial function. For example, perhaps age-related accumulations of a variety of protein aggregates like amyloid as well as myelin debris overburden microglia. Alternatively, perhaps microglia functionality simply declines with age, allowing damage to go unresolved? These questions must be considered not only in aging, but also in neurodegenerative diseases where debris clearance could play a key role in disease progression. Further, as the leading risk factor for neurodegenerative diseases is age (Mayeux and Stern 2012), it is possible that the burden of myelin debris may play a role in the ability of microglia to deal with other damage in the brain, such as amyloid plaques, phosphorylated tau oligomers, or  $\alpha$ -synuclein aggregates.

#### Autophagy and aging

While phagocytosis is important for the clearance of cellular debris, autophagy is the process required for normal maintenance of cellular function through breakdown of intracellular debris (Glick et al. 2010). Data indicate that inhibiting autophagy in mice decreases lifespan and increases protein aggregation (Hara et al. 2006; Komatsu et al. 2006). In contrast, increasing autophagy in worms (Hansen et al. 2008) and flies (Simonsen et al. 2008) extends lifespan. Interestingly, calorie restriction without malnutrition increases autophagy in rats (Kume et al. 2010) and extends life span (Weindruch and Walford 1982) and monkeys (Mattison et al. 2017). While the exact mechanism by which calorie restriction enhances autophagy is unclear, it is thought to involve AMPK or Sirtuin 1 stimulation or insulin-like growth factor inhibition (Johnson et al. 2013). Although both autophagy and phagocytosis show age-related functional changes, little is known about possible linkage between these clearance mechanisms. Additionally, it is unknown why these

mechanisms for degradation become faulty with age and whether these changes occur in monkeys.

#### Cognitive decline and phagocytosis

While the density of LN3+ and Gal-3+ microglia increase significantly with age, it is curious that Gal-3+ cell density in the FWM was the only strong correlate with cognitive impairment. While some have reported that cognitive impairment is predicted best by total frontal white matter (Tullberg et al. 2004, Wakefield et al. 2010), others have claimed that regional specificity is important (Bowley et al. 2010, Head 2004, Mielke et al. 2009). Bowley et al. (2010) showed that myelin defects are specifically correlated with cognitive decline in the cingulum, but not the corpus callosum. However, DTI data from Mielke et al. (2009) and Head (2004) suggest that frontal white matter damage, but not temporal or occipital, correlate with cognitive performance. The specificity of the current finding of a relationship of Gal-3 with cognitive impairment only in FWM could suggest that myelin damage was more severe in this area, leading to more microglia being primed for phagocytosis but ultimately ineffective in allowing remyelination. This is consistent with our additional observation that within the FWM, the density of both hypertrophic (activated) and amoeboid (phagocytic) Gal-3+ cells correlated with cognitive decline while the density of ramified (resting) microglia did not. It further suggests that these microglia are not functioning properly and allow myelin damage to accumulate, leading to an increase in the number of microglia recruited and activated and a continuation of the inflammatory response. The specificity of this finding to the FWM might indicate especially faulty clearance mechanisms in this region, i.e., a particular vulnerability. However, it is possible that Gal-3+ microglia are simply acting as a surrogate marker for the overall white matter damage and general aging dysfunction. Understanding the regional differences in myelin damage and age-related pathologies is essential to determining the relation of inflammation to and the causes of age-related cognitive decline.

#### Conclusions

During aging, myelin deteriorates and appears to be a strong predictor of the age-related cognitive decline seen

in normal aging (Bartzokis 2004; Peters 2009). As the myelin debris accumulates, it likely leads to the increased recruitment of the activated and phagocytic microglia observed in the present study. In a healthy adult, this would trigger an acute inflammatory response supporting microglial phagocytosis and clearance of the debris, resolving with oligodendrocyte precursor cell differentiation and remyelination. However, with aging, the capacity of microglia to clear the myelin debris likely declines as shown by Plowden et al. (2004) and Safaiyan et al. (2016), leaving microglia unable to effectively respond to the damage and remyelination impeded by inhibition of oligodendrocyte differentiation. Similar phagocytic inefficiencies may also contribute to the vulnerability of the brain to age-related neurodegenerative diseases. Thus, therapeutics targeting the phagocytic functionality of aging microglia could prove useful not only in facilitating remyelination, and slowing or even reversing age-related cognitive decline, but might also be valuable in treating age-related neurodegenerative diseases.

**Acknowledgements** We would like to acknowledge our technicians and staff, without whom these studies would not be possible: Bethany Bowley, Alana Carmichael, Simrat Dhaliwal, Penny Schultz, Karen L. Slater, and Rebecca Smith. This work was supported by NIH grants R01-AG043640 and NIH R01-AG042512.

## References

- Albert M (1993) Neuropsychological and neurophysiological changes in healthy adult humans across the age range. *Neurobiol Aging* 14:623–625. doi:10.1016/0197-4580(93)90049-H
- Alexander GE, Chen K, Merkley TL et al (2006) Regional network of magnetic resonance imaging gray matter volume in healthy aging. *Neuroreport* 17:951–956. doi:10.1097/01.wnr.0000220135.16844.b6
- Bartzokis G (2004) Age-related myelin breakdown: a developmental model of cognitive decline and Alzheimer's disease. *Neurobiol Aging* 25:5–18
- Bohatschek M, Kloss CUA, Kalla R, Raivich G (2001) In vitro model of microglial deramification: ramified microglia transform into amoeboid phagocytes following addition of brain cell membranes to microglia-astrocyte cocultures. *J Neurosci Res* 64:508–522. doi:10.1002/jnr.1103
- Bowley MP, Cabral H, Rosene DL, Peters A (2010) Age changes in myelinated nerve fibers of the cingulate bundle and corpus callosum in the rhesus monkey. *J Comp Neurol* 518:3046–3064. doi:10.1002/cne.22379
- Brück W, Brück Y, Friede RL (1992) TNF-alpha suppresses CR3-mediated myelin removal by macrophages. *J Neuroimmunol* 38:9–17. doi:10.1016/0165-5728(92)90085-Y
- Cherry JD, Olschowka JA, O'Banion MK (2014) Neuroinflammation and M2 microglia: the good, the bad, and the inflamed. *J Neuroinflammation* 11:98. doi:10.1186/1742-2094-11-98
- Chung H, Brazil MI, Soe TT, Maxfield FR (1999) Uptake, degradation, and release of fibrillar and soluble forms of Alzheimer's amyloid B-peptide by microglial cells. *J Biol Chem* 274:32301–32308. doi:10.1074/jbc.274.45.32301
- Conde JR, Streit WJ (2006) Microglia in the aging brain. *J Neuropathol Exp Neurol* 65:199–203. doi:10.1097/01.jnen.0000202887.22082.63
- Cribbs DH, Berchtold NC, Perreau V et al (2012) Extensive innate immune gene activation accompanies brain aging, increasing vulnerability to cognitive decline and neurodegeneration: a microarray study. *J Neuroinflammation* 9:179. doi:10.1186/1742-2094-9-179
- DiPatre PL, Gelman BB (1997) Microglial cell activation in aging and Alzheimer disease: partial linkage with neurofibrillary tangle burden in the hippocampus. *J Neuropathol Exp Neurol* 56:143–149
- Dumic J, Dabelic S, Flögel M (2006) Galectin-3: an open-ended story. *Biochim Biophys Acta* 1760:616–635. doi:10.1016/j.bbagen.2005.12.020
- Elliott MJ, Strasser A, Metcalf D (1991) Selective up-regulation of macrophage function in granulocyte-macrophage colony-stimulating factor transgenic mice. *J Immunol* 147:2957–2963
- Feldman ML, Peters A (1998) Ballooning of myelin sheaths in normally aged macaques. *J Neurocytol* 27:605–614. doi:10.1023/A:1006926428699
- Gallagher M, Burwell RD (1989) Relationship of age-related decline across several behavioral domains. *Neurobiol Aging* 10:691–708. doi:10.1016/0197-4580(89)90006-7
- Gardner ID, Lim STK, Lawton JWM (1981) Monocyte function in ageing humans. *Mech Ageing Dev* 16:233–239. doi:10.1016/0047-6374(81)90099-3
- Glick D, Barth S, Macleod K (2010) Autophagy: cellular and molecular mechanisms. *J Pathol* 221:3–12. doi:10.1002/path.2697
- Gordon S, Martinez FO (2010) Alternative activation of macrophages: mechanism and functions. *Immunity* 32:593–604
- Gundersen HJG, Jensen EBV, Kiøu K, Nielsen J (1999) The efficiency of systematic sampling in stereology—reconsidered. *J Microsc* 193:199–211. doi:10.1046/j.1365-2818.1999.00457.x
- Guttmann CR, Jolesz FA, Kikinis R et al (1998) White matter changes with normal aging. *Neurology* 50:972–978. doi:10.1212/WNL.50.4.972
- Hansen M, Chandra A, Mitic LL et al (2008) A role for autophagy in the extension of lifespan by dietary restriction in *C. elegans*. *PLoS Genet*. doi:10.1371/journal.pgen.0040024
- Hara T, Nakamura K, Matsui M et al (2006) Suppression of basal autophagy in neural cells causes neurodegenerative disease in mice. *Nature* 441:885–889. doi:10.1038/nature04724
- Hart AD, Wytenbach A, Hugh Pery V, Teeling JL (2012) Age related changes in microglial phenotype vary between CNS regions: Grey versus white matter differences. *Brain Behav Immun* 26:754–765. doi:10.1016/j.bbi.2011.11.006
- Head D (2004) Differential vulnerability of anterior white matter in nondemented aging with minimal acceleration in dementia of the Alzheimer type: evidence from diffusion tensor imaging. *Cereb Cortex* 14:410–423. doi:10.1093/cercor/bhh003

- Henry CJ, Huang Y, Wynne AM, Godbout JP (2009) Peripheral lipopolysaccharide (LPS) challenge promotes microglial hyperactivity in aged mice that is associated with exaggerated induction of both pro-inflammatory IL-1 $\beta$  and anti-inflammatory IL-10 cytokines. *Brain Behav Immun* 23: 309–317. doi:10.1016/j.bbi.2008.09.002
- Herndon JG, Moss MB, Rosene DL, Killiany RJ (1997) Patterns of cognitive decline in aged rhesus monkeys. *Behav Brain Res* 87:25–34. doi:10.1016/S0166-4328(96)02256-5
- Hickman SE, El Khoury J (2014) TREM2 and the neuroimmunology of Alzheimer's disease. *Biochem Pharmacol* 88:495–498. doi:10.1016/j.bcp.2013.11.021
- Hoffman GE, Murphy KJ, Sita LV (2016) The importance of titrating antibodies for immunocytochemical methods. *Curr Protoc Neurosci* 76:2.12.1–2.12.37. doi:10.1002/cpns.1
- Holtman IR, Raj DD, Miller JA et al (2015) Induction of a common microglia gene expression signature by aging and neurodegenerative conditions: a co-expression meta-analysis. *Acta Neuropathol Commun* 3. doi:10.1186/s40478-015-0203-5
- Hoyos HC, Rinaldi M, Mendez-Huergo SP et al (2014) Galectin-3 controls the response of microglial cells to limit cuprizone-induced demyelination. *Neurobiol Dis* 62:441–455. doi:10.1016/j.nbd.2013.10.023
- Johnson SC, Rabinovitch PS, Kaeberlein M (2013) mTOR is a key modulator of ageing and age-related disease. *Nature* 493: 338–345. doi:10.1038/nature11861
- Karperien A, Ahammer H, Jelinek HF (2013) Quantitating the subtleties of microglial morphology with fractal analysis. *Front Cell Neurosci* 7:3. doi:10.3389/fncel.2013.00003
- Kay JG, Murray RZ, Pagan JK, Stow JL (2006) Cytokine secretion via cholesterol-rich lipid raft-associated SNAREs at the phagocytic cup. *J Biol Chem* 281:11949–11954. doi:10.1074/jbc.M600857200
- Kohama SG, Rosene DL, Sherman LS (2011) Age-related changes in human and non-human primate white matter: from myelination disturbances to cognitive decline. *Age (Dordr)* 34:1093–1110. doi:10.1007/s11357-011-9357-7
- Komatsu M, Waguri S, Chiba T et al (2006) Loss of autophagy in the central nervous system causes neurodegeneration in mice. *Nature* 441:880–884. doi:10.1038/nature04723
- Koo B, Schettler S, Murray D, Lee J (2010) Age-related effects on cortical thickness patterns of the rhesus monkey brain. *Neurobiol Aging* 33:200.e23–31. doi:10.1016/j.neurobiolaging.2010.07.010
- Kotter MR, Li W-W, Zhao C, Franklin RJM (2006) Myelin impairs CNS remyelination by inhibiting oligodendrocyte precursor cell differentiation. *J Neurosci* 26:328–332. doi:10.1523/JNEUROSCI.2615-05.2006
- Kotter MR, Zhao C, Van Rooijen N, Franklin RJM (2005) Macrophage-depletion induced impairment of experimental CNS remyelination is associated with a reduced oligodendrocyte progenitor cell response and altered growth factor expression. *Neurobiol Dis* 18:166–175. doi:10.1016/j.nbd.2004.09.019
- Kume S, Uzu T, Horiike K et al (2010) Calorie restriction enhances cell adaptation to hypoxia through Sirt1-dependent mitochondrial autophagy in mouse aged kidney. *J Clin Invest* 120:1043–1055. doi:10.1172/JCI41376
- Lampron A, Laroche A, Laflamme N et al (2015) Inefficient clearance of myelin debris by microglia impairs remyelinating processes. *J Exp Med* 212:481–495. doi:10.1084/jem.20141656
- Lee JE, Liang KJ, Fariss RN, Wong WT (2008) Ex vivo dynamic imaging of retinal microglia using time-lapse confocal microscopy. *Investig Ophthalmol Vis Sci* 49:4169–4176. doi:10.1167/iov.08-2076
- Leverrier Y, Ridley AJ (2001) Requirement for Rho GTPases and PI 3-kinases during apoptotic cell phagocytosis by macrophages. *Curr Biol* 11:195–199. doi:10.1016/S0960-9822(01)00047-1
- Linehan E, Dombrowski Y, Snoddy R et al (2014) Aging impairs peritoneal but not bone marrow-derived macrophage phagocytosis. *Aging Cell* 13:699–708. doi:10.1111/acel.12223
- Liu Y, Hao W, Letiembre M et al (2006) Suppression of microglial inflammatory activity by myelin phagocytosis: role of p47-PHOX-mediated generation of reactive oxygen species. *J Neurosci* 26:12904–12913. doi:10.1523/JNEUROSCI.2531-06.2006
- Lucin KM, O'Brien CE, Bieri G et al (2013) Microglial beclin 1 regulates retromer trafficking and phagocytosis and is impaired in Alzheimer's disease. *Neuron* 79:873–886. doi:10.1016/j.neuron.2013.06.046
- Makris N, Papadimitriou GM, van der Kouwe A et al (2007) Frontal connections and cognitive changes in normal aging rhesus monkeys: a DTI study. *Neurobiol Aging* 28:1556–1567. doi:10.1016/j.neurobiolaging.2006.07.005
- Marnier L, Nyengaard JR, Tang Y, Pakkenberg B (2003) Marked loss of myelinated nerve fibers in the human brain with age. *J Comp Neurol* 462:144–152. doi:10.1002/cne.10714
- Martinez FO, Gordon S (2014) The M1 and M2 paradigm of macrophage activation: time for reassessment. *F1000Prime Rep* 6:13. doi:10.12703/P6-13
- Mattison JA, Colman RJ, Beasley TM et al (2017) Caloric restriction improves health and survival of rhesus monkeys. *Nat Commun* 8:14063. doi:10.1038/ncomms14063
- Mayeux R, Stern Y (2012) Epidemiology of Alzheimer disease. *Cold Spring Harb Perspect Med* 2:137–152. doi:10.1101/cshperspect.a006239
- Merrill DA, Roberts JA, Tuszyński MH (2000) Conservation of neuron number and size in entorhinal cortex layers II, III, and V/VI of aged primates. *J Comp Neurol* 422:396–401. doi:10.3389/neuro.05.011.2009
- Mielke MM, Kozauer NA, Chan KCG et al (2009) Regionally-specific diffusion tensor imaging in mild cognitive impairment and Alzheimer's disease. *NeuroImage* 46:47–55. doi:10.1016/j.neuroimage.2009.01.054
- Mittelbronn M, Dietz K, Schluesener HJ, Meyermann R (2001) Local distribution of microglia in the normal adult human central nervous system differs by up to one order of magnitude. *Acta Neuropathol* 101:249–255
- Moore TL, Schettler SP, Killiany RJ et al (2005) Cognitive impairment in aged rhesus monkeys associated with monoamine receptors in the prefrontal cortex. *Behav Brain Res* 160:208–221. doi:10.1016/j.bbr.2004.12.003
- Moss MB, Moore TL, Schettler SP, et al. (2007) Successful vs. unsuccessful aging in the rhesus monkey. In: *Brain aging: models, methods, and mechanisms*. pp 21–38
- Murray RZ, Kay JG, Sangermani DG, Stow JL (2005) A role for the phagosome in cytokine secretion. *Science* 310:1492–1495. doi:10.1126/science.1120225

- Natrajan MS, De La Fuente AG, Crawford AH et al (2015) Retinoid X receptor activation reverses age-related deficiencies in myelin debris phagocytosis and remyelination. *Brain* 138:3581–3597. doi:10.1093/brain/awv289
- Neumann H, Kotter MR, Franklin RJM (2009) Debris clearance by microglia: an essential link between degeneration and regeneration. *Brain* 132:288–295
- Nimmerjahn A, Kirchhoff F, Helmchen F (2005) Resting microglial cells are highly dynamic surveillants of brain parenchyma in vivo. *Neuroforum* 11:95–96. doi:10.1126/science.1110647
- Norden DM, Godbout JP (2013) Review: microglia of the aged brain: primed to be activated and resistant to regulation. *Neuropathol Appl Neurobiol* 39:19–34
- Park DC, Reuter-Lorenz P (2009) The adaptive brain: aging and neurocognitive scaffolding. *Annu Rev Psychol* 60:173–196. doi:10.1146/annurev.psych.59.103006.093656
- Paxinos G, Huang XF, Toga AW (2000) The rhesus monkey brain in stereotaxic coordinates. Academic Press, San Diego
- Perry VH, Holmes C (2014) Microglial priming in neurodegenerative disease. *Nat Rev Neurol* 10:217–224. doi:10.1038/nrneurol.2014.38
- Peters A (1996) Age-related changes in oligodendrocytes in monkey cerebral cortex. *J Comp Neurol* 371:153–163. doi:10.1002/(SICI)1096-9861(19960715)371:1<153:AID-CNE9>3.0.CO;2-2
- Peters A (2009) The effects of normal aging on myelinated nerve fibers in monkey central nervous system. *Front Neuroanat* 3:11. doi:10.3389/neuro.05.011.2009
- Peters A, Kemper T (2012) A review of the structural alterations in the cerebral hemispheres of the aging rhesus monkey. *Neurobiol Aging* 33:2357–2372
- Peters A, Morrison JH, Rosene DL, Hyman BT (1998) Are neurons lost from the primate cerebral cortex during normal aging? *Cereb. Cortex* 8:295–300
- Peters A, Moss MB, Sethares C (2000) Effects of aging on myelinated nerve fibers in monkey primary visual cortex. *J Comp Neurol* 419:364–376. doi:10.1002/(SICI)1096-9861(20000410)419:3<364::AID-CNE8>3.0.CO;2-R
- Peters A, Rosene DL (2003) In aging, is it gray or white? *J Comp Neurol* 462:139–143. doi:10.1002/cne.10715
- Peters A, Sethares C (2002) Aging and the myelinated fibers in prefrontal cortex and corpus callosum of the monkey. *J Comp Neurol* 442:277–291. doi:10.1002/cne.10099
- Peters A, Sethares C, Moss MB (2010) How the primate fornix is affected by age. *J Comp Neurol* 518:3962–3980. doi:10.1002/cne.22434
- Plowden J, Renshaw-Hoelscher M, Engleman C et al (2004) Innate immunity in aging: impact on macrophage function. *Aging Cell* 3:161–167. doi:10.1111/j.1474-9728.2004.00102.x
- Prinz M, Priller J (2014) Microglia and brain macrophages in the molecular age: from origin to neuropsychiatric disease. *Nat Rev Neurosci* 15:300–312. doi:10.1038/nrn3722
- Pugliese G, Iacobini C, Pesce CM, Menini S (2015) Galectin-3: an emerging all-out player in metabolic disorders and their complications. *Glycobiology* 25:136–150. doi:10.1093/glycob/cwu111
- Ransohoff RM (2016) A polarizing question: do M1 and M2 microglia exist? *Nat Neurosci* 19:987–991. doi:10.1038/nn.4338
- Rawji KS, Mishra MK, Michaels NJ, Rivest S, Stys PK, Yong VW (2016) Immunosenescence of microglia and macrophages: impact on the ageing central nervous system. *Brain* 139 (3): 653–661. doi:10.1093/brain/awv395
- Reichert F, Rotshenker S (1999) Galectin-3/MAC-2 in experimental allergic encephalomyelitis. *Exp Neurol* 160:508–514. doi:10.1006/exnr.1999.7229
- Rogers J, Lubner-Narod J, Styren SD, Civin WH (1988) Expression of immune system-associated antigens by cells of the human central nervous system: relationship to the pathology of Alzheimer's disease. *Neurobiol Aging* 9:339–349. doi:10.1016/S0197-4580(88)80079-4
- Rosene DL, Roy NJ, Davis BJ (1986) A cryoprotection method that facilitates cutting frozen sections of whole monkey brains for histological and histochemical processing without freezing artifact. *J Histochem Cytochem* 34:1301–1315. doi:10.1177/34.10.3745909
- Rozovsky I, Finch CE, Morgan TE (1998) Age-related activation of microglia and astrocytes: in vitro studies show persistent phenotypes of aging, increased proliferation, and resistance to down-regulation. *Neurobiol Aging* 19:97–103
- Ruckh JM, Zhao JW, Shadrach JL et al (2012) Rejuvenation of regeneration in the aging central nervous system. *Cell Stem Cell* 10:96–103. doi:10.1016/j.stem.2011.11.019
- Safaiyan S, Kannaiyan N, Snaidero N et al (2016) Age-related myelin degradation burdens the clearance function of microglia during aging. *Nat Neurosci* 19:995–998. doi:10.1038/nn.4325
- Sandell JH, Peters A (2003) Disrupted myelin and axon loss in the anterior commissure of the aged rhesus monkey. *J Comp Neurol* 466:14–30. doi:10.1002/cne.10859
- Sandell JH, Peters A (2002) Effects of age on the glial cells in the rhesus monkey optic nerve. *J Comp Neurol* 445:13–28. doi:10.1002/cne.10162
- Sano H, Hsu DK, Apgar JR, et al. (2003) Critical role of galectin-3 in phagocytosis by macrophages. *J Clin Invest* 112:389–397. doi:10.1172/JCI200317592
- Sheffield LG, Berman NE (1998) Microglial expression of MHC class II increases in normal aging of nonhuman primates. *Neurobiol Aging* 19:47–55
- Sierra A, Gottfried-blackmore AC, McEwen BS (2007) Microglia derived from aging mice exhibit an altered inflammatory profile. *Glia* 424:412–424. doi:10.1002/glia.20468
- Simonsen A, Cumming RC, Brech A et al (2008) Promoting basal levels of autophagy in the nervous system enhances longevity and oxidant resistance in adult *Drosophila*. *Autophagy* 4:176–184. doi:10.4161/auto.5269
- Sloane JA, Hollander W, Moss MB et al (1999) Increased microglial activation and protein nitration in white matter of the aging monkey. *Neurobiol Aging* 20:395–405
- Sloane JA, Pietropaolo MF, Rosene DL et al (1997) Lack of correlation between plaque burden and cognition in the aged monkey. *Acta Neuropathol* 94:471–478. doi:10.1007/s004010050735
- Streit WJ, Sammons NW, Kuhns AJ, Sparks DL (2004) Dystrophic microglia in the aging human brain. *Glia* 45:208–212. doi:10.1002/glia.10319
- Streit WJ, Sparks DL (1997) Activation of microglia in the brains of humans with heart disease and hypercholesterolemic rabbits. *J Mol Med* 75:130–138. doi:10.1007/s001090050097
- Tang Y, Le W (2015) Differential roles of M1 and M2 microglia in neurodegenerative diseases. *Mol Neurobiol* 53:1181–1194. doi:10.1007/s12035-014-9070-5

- Tang Y, Nyengaard JR, Pakkenberg B, Gundersen HJ (1997) Age-induced white matter changes in the human brain: a stereological investigation. *Neurobiol Aging* 18:609–615. doi:[10.1016/S0197-4580\(97\)00155-3](https://doi.org/10.1016/S0197-4580(97)00155-3)
- Tigges J, Gordon TP, McClure HM et al (1988) Survival rate and life span of rhesus monkeys at the Yerkes Regional Primate Research Center. *Am J Primatol* 15:263–273
- Ting JP-Y, Trowsdale J (2002) Genetic control of MHC class II expression. *Cell* 109(Suppl):S21–S33. doi:[10.1016/S0092-8674\(02\)00696-7](https://doi.org/10.1016/S0092-8674(02)00696-7)
- Town T, Nikolic V, Tan J (2005) The microglial “activation” continuum: from innate to adaptive responses. *J Neuroinflammation* 2:24. doi:[10.1186/1742-2094-2-24](https://doi.org/10.1186/1742-2094-2-24)
- Tullberg M, Fletcher E, DeCarli C, Mungas D, Reed BR, Harvey DJ, Weiner MW, Chui HC, Jagust WJ (2004) White matter lesions impair frontal lobe function regardless of their location. *Neurology* 63 (2):246–253
- Wakefield DB, Moscufo N, Guttmann CR, Kuchel GA, Kaplan RF, Pearlson G, Wolfson L (2010) White matter hyperintensities predict functional decline in voiding, mobility, and cognition in older adults. *J Am Geriatr Soc* 58 (2): 275–281. doi:[10.1111/j.1532-5415.2009.02699.x](https://doi.org/10.1111/j.1532-5415.2009.02699.x)
- Weindruch R, Walford RL (1982) Dietary restriction in mice beginning at 1 year of age: effect on life-span and spontaneous cancer incidence. *Science* 215:1415–1418. doi:[10.1126/science.7063854](https://doi.org/10.1126/science.7063854)
- West MJ, Slomianka L, Gundersen HJ (1991) Unbiased stereological estimation of the total number of neurons in the subdivisions of the rat hippocampus using the optical fractionator. *Anat Rec* 231: 482–497. doi:[10.1002/ar.1092310411](https://doi.org/10.1002/ar.1092310411)
- Williams K, Ulvestad E, Waage A et al (1994) Activation of adult human derived microglia by myelin phagocytosis in vitro. *J Neurosci Res* 38:433–443. doi:[10.1002/jnr.490380409](https://doi.org/10.1002/jnr.490380409)
- Wisco JJ, Killiany RJ, Guttmann CRG et al (2008) An MRI study of age-related white and gray matter volume changes in the rhesus monkey. *Neurobiol Aging* 29:1563–1575. doi:[10.1016/j.neurobiolaging.2007.03.022](https://doi.org/10.1016/j.neurobiolaging.2007.03.022)